Studies in Fungi

ARTICLE

Open Access

https://doi.org/10.48130/sif-0025-0018
Studies in Fungi **2025**, 10: e018

Biosorption of zinc ions (Zn^{2+}) by dead *Aspergillus flavus* link mycomass: isotherm, kinetics, and thermodynamic studies

Amit Kumar[1*], Raj Singh[2], Ashu Tyagi[3], Pradip Kumar[3] and Permod Kumar[4]

[1] *Department of Botany, Keral Verma Subharti College of Science, Swami Vivekananda Subharti University, Meerut, Uttar Pradesh, India*
[2] *Department of Bio-Sciences and Technology, Maharshi Markandeshvar (deemed to be University), Mullana, Ambala, Haryana, India*
[3] *Depart of Biotechnology, CCS University, Meerut, Uttar Pradesh, India*
[4] *Department of Botany, Dhnauri PG College Dhanauri, Haridwar, Uttrakhand, India*
* Corresponding author, E-mail: amitsaini.saini421@gmail.com

Abstract

The present study explores the potential of dead *Aspergillus flavus* mycomass (DAFM) as an effective, eco-friendly, and low-cost myco-biosorbent for the removal of Zn^{2+} ions from contaminated aqueous environments. DAFM, characterized by its chemically diverse surface and abundance of functional groups, offers significant promise for the removal of metal ions. The study systematically optimized key operational parameters – including biomass age, particle size, temperature, contact time, DAFM dosage, and initial Zn^{2+} concentration – to identify the most favorable conditions for maximum biosorptive efficiency. Advanced characterization techniques, including FT-IR spectroscopy, confirmed the active participation of functional moieties such as hydroxyl, carboxyl, and amide groups in Zn^{2+} binding, underscoring the role of physicochemical interactions in the adsorption process. The maximum adsorption capacity (q_{max} = 65.69 mg·g^{-1}) obtained with Langmuir's isotherm model exhibited a close relationship with experimental adsorption capacity. Kinetic analysis supported the pseudo-second-order model, indicating chemisorption as the dominant mechanism, while thermodynamic evaluation revealed that the process is spontaneous and endothermic, with increased randomness at the solid-liquid interface. Furthermore, equilibrium modeling demonstrated the system's conformity to the Langmuir isotherm, highlighting the monolayer adsorption capacity of DAFM. Overall, the findings affirm the potential utility of DAFM in industrial effluent treatment, particularly in sectors releasing zinc-laden wastewater. This study lays the groundwork for scalable applications of fungal biomass in biosorption technologies, contributing to the development of sustainable and cost-effective water purification systems suitable for use in resource-limited settings.

Citation: Kumar A, Singh R, Tyagi A, Kumar P, Kumar P. 2025. Biosorption of zinc ions (Zn^{2+}) by dead *Aspergillus flavus* link mycomass: isotherm, kinetics, and thermodynamic studies. *Studies in Fungi* 10: e018 https://doi.org/10.48130/sif-0025-0018

Introduction

Zinc is one of the most extensively used and toxic heavy metals. The World Health Organization has recommended that the maximum acceptable concentration of zinc is 0.05 mg·L^{-1} in surface and ground water. The concentration level of zinc is increasing steadily in the environment. Zn^{2+} is a micronutrient necessary to all living things[1]. The excessive intake of Zn^{2+} can however be fatal, and it accumulates in the body of the organisms through the food chain via bio-geochemical cycles[2,3]. According to the United States Environmental Protection Agency (USEPA), Zn^{2+} has been ranked in the list of toxic heavy metals[4,5]. The limit of discharge of Zn^{2+} in ground water, fresh water, and estuaries recorded by government agencies of various countries is shown in Table 1. The Comprehensive Environmental Response, Compensation, and Liability Act-2007 (CERCLA) has ranked Zn^{2+} 74th with respect to water pollution[6]. Hussain et al.[7] suggested that the utility, as well as deficiency and toxicity effects of Zn^{2+}, are enough to develop awareness towards maintenance and mitigation of this precious metal.

The mitigation of heavy metals, including Zn^{2+} to the optimal level is crucial. To achieve this, several strategies such as physical and chemical techniques have been in use, including ion-exchange[13], ion floatation[14], electro-coagulation/floatation[15,16], electro-deposition[17], irradiation[18], ozonation[19], adsorption though the use of activated carbon[20], precipitation/sedimentation[21], biological operations like microbial fuel cells[22], flocculation[23], filtration through membranes[24], chemical precipitation[25], and solvent extraction[26].

However, all of these methods have proven to be quite effective for the removal of heavy metals but they have many operational difficulties, including the production of concentrated sludge that creates a secondary disposal problem and thus, are considered to be expensive. Therefore, biological processes, such as biodegradation, bioaccumulation, or biosorption, have received increasing interest due to their low cost, effectiveness, ability to produce less or no sludge, and environmental benignity[27].

In the current scenario, biosorption is attracting the attention of environmental researchers. It involves the removal of pollutants from aqueous solution using biological materials or their derivatives. A number of studies have already been published on the biosorption of metals using different biological agents as adsorbents. These include the phytomass of algae, lichens, bryophytes, pteridophytes, angiosperms[28–32], egg shell[33], agricultural waste[34], agro-industrial waste[35], bacteria[27], and fungi[36]. Fungal biomass, due to its excellent biosorptive potential, have been in use as a cheap source of biosorbent, along with some advantages over other conventional adsorbents. Dead mycomass offers excellent utility over a living one due to multiple reasons: (i) no toxicity; (ii) excellent performance in removal of pollutants; (iii) operational ease and low cost; (iv) no requirement for a regular nutrient supply; (v) no production of bio-chemical sludge; and (vi) reusability for numerous cycles.

Recently the mycomass of many fungal species has been tried for metal biosorption, mainly involving the *Aspergillus*[36], *Rhizopus*[37], *Penicillium*[38], *Trichoderma aspergillus*[39], *Streptoverticillum*[40], and *Sacharomyces*[41]. Therefore, the present study was formulated for

Table 1. Discharge limit of Zn^{2+} suggested by various government agencies.

Name of the agency	Type of water	Discharge limit ($mg \cdot L^{-1}$)	Ref.
World Health Organization (WHO)	Drinking water	5	[4,8,9]
Minimum National Standards (MINAS), Ministry of Environment and Forest, Government of India	Surface water	5	[10]
Minimum National Standards (MINAS), Ministry of Environment and Forest, Government of India	Potable water	3	[11]
Central Pollution Control Board, India	Wastewater	5	[12]
United States Environment Protection Agency	Drinking water	5	

the biosorption of Zn^{2+} by dead mycomass of *Aspergillus flavus* (DAFM). For achieving the maximum removal under a fabricated water-treatment system, the present research aimed to investigate the potential of DAFM to adsorb Zn^{2+} from its aqueous solution. For the optimization of conditions, the biosorption experiments were performed under different ranges of parameters including contact time, temperature, mycomass dose, mycomass particle size, and initial dye concentration. The effect of pH was not examined because neutral pH (pH = 7.0) has been reported to be effective for Zn^{2+} removal[36]. The experimental data were evaluated by fitting into different isotherm models. For a better understanding of the nature of Zn^{2+} biosorption, the experimental data was evaluated via thermodynamic studies. Besides these, to understand the biosorption mechanism, the biosorption data were evaluated using different kinetic models. The functional groups present on the DAFM surface were investigated through FTIR spectroscopy of DAFM, before and after biosorption.

The present investigation was hypothesized for the biosorption of zinc using the biomass of dead *Aspergillus flavus* mycelia. It is a sustainable and cost-effective strategy for the removal of Zn^{2+} metal ions from contaminated water. The core hypothesis is that the fungal biomass, owing to the presence of active functional groups such as carboxyl, amine, amide, hydroxyl, phosphate, and amino groups on its cell wall, can effectively adsorb Zn^{2+} ions through mechanisms like ion exchange, complexation, and chemical and physical adsorption. The objective of this research is to investigate the metal-binding efficiency of DAFM under different environmental and operational parameters, including: DAFM particle size DAFM age, temperature, contact duration, initial zinc concentration, and DAFM dosage. This research also aims to model the biosorption process using adsorption isotherms and kinetic models to understand the nature of metal uptake. Furthermore, it seeks to evaluate the thermodynamic behavior of the process. Overall, the study is directed toward establishing *Aspergillus flavus* as a viable biosorbent for zinc decontamination in industrial wastewater, offering a greener alternative to conventional remediation techniques.

Materials and methods

Selection of *Aspergillus flavus* as a biosorbent and the preparation of DAFM

In the present study, the fungus *A. flavus,* chosen for the preparation of mycomass, was isolated from soil samples[42], and selected on the basis of its dominance for biosorption of Zn^{2+}. The mycelial mycomass of *A. flavus* was prepared on liquid MGYP medium after sterilization at 15 psi, 121 °C for 15 min. For the preparation of *A. flavus* mycomass, the inoculum was added to five flasks containing MGYP broth. After 96 h of incubation at 25 ± 2 °C in a BOD incubator shaker, all the flasks were steam sterilized in an autoclave. The dead mycelial mat of *A. flavus* was then harvested by filtering through a standard sieve. The mycomass was then washed twice with double-distilled water and the obtained mycelial biomass was then placed into a hot air oven for drying at 60 ± 2 °C for 24 h. The dried and dead *A. flavus* mycomass was then crushed using a mortar and pestle to achieve fine powdered mycomass. The mycomass was then filtered via standard sieves to obtain the mycomass of three different particle size, i.e., 125–250, 250–355, and 355–500 μm.

Preparation of Zn^{2+} solutions of different concentrations

Zinc sulphate powder was added to distilled water to obtain zinc solutions of different concentrations to assess the Zn^{2+} removal ability of DAFM. The stock solutions of metal (Zn^{2+}) were prepared to obtain different concentrations (100, 200, 300, 400, and 500 ppm) separately.

Biosorption of Zn^{2+} by DAFM

A set of 27 flasks of 250 mL capacity, filled with 100 mL of 100 ppm zinc solution (as zinc sulphate) were used for given mycomass, i.e., DAFM, for determining the effect of mycomass age and particle size on biosorption of Zn^{2+}. The 27 flasks was divided into three subsets, each for different mycomass ages (subset I of 48 h, II for 96 h, and III for 144 h age of DAFM). To the nine flasks of subset I, DAFM was added as follows:

Set 1:

A:

(i) 10 mg DAFM (of 48 h age and 355–500 μm particle size) + 100 ppm zinc sulphate solution: three flasks;

(ii) 10 mg DAFM (of 48 h age and 250–355 μm particle size) + 100 ppm zinc sulphate solution: three flasks;

(iii) 10 mg DAFM (of 48 h age and 125–250 μm particle size) + 100 ppm zinc sulphate solution: three flasks.

Similarly, the DAFM was added to subset II and III as:

B:

(i) 10 mg DAFM (of 96 h age and 355–500 μm particle size) + 100 ppm zinc sulphate solution: three flasks;

(ii) 10 mg DAFM (of 96 h age and 250–355 μm particle size) + 100 ppm zinc sulphate solution: three flasks;

(iii) 10 mg DAFM (of 96 h age and 125–250 μm particle size) + 100 ppm zinc sulphate solution: three flasks.

C:

(i) 10 mg DAFM (of 144 h age and 355–500 μm particle size) + 100 ppm zinc sulphate solution: three flasks;

(ii) 10 mg DAFM (of 144 h age and 250–355 μm particle size) + 100 ppm zinc sulphate solution: three flasks;

(iii) 20 mg DAFM (of 144 h age and 125–250 μm particle size) + 100 ppm zinc sulphate solution: three flasks.

A set of three flasks containing 100 ppm zinc solution, without added DAFM served as control. All flasks were then placed on a rotator shaker at 150 rpm for 20 min. After a contact period of 20 min, the mycomass was separated by filtering the reaction mixture through a Whatman No. 40 filter paper to prevent the probable interference of turbidity and the filtrate was further processed for assessing the concentration of metal remaining in the solution. A few drops of concentrated nitric acid and hydrochloric acid were added in the filtrate for the acidification. Thereafter, the sets of three flasks of a particular particle size within a particular age mycomass were pooled together to achieve a composite solution for atomic absorption spectrophotometery. Before the measurement, the filtrates were diluted with appropriate amounts of double-distilled water. The absorbance of these were recorded on an AA-7000 model atomic absorption spectrophotometer (AAS).

Another set of 15 flasks were used for the determination of optimal contact time for the removal of Zn^{2+} using DAFM. These 15

flasks were divided into five subsets of three flasks for 20 min, 40 min, 60 min, 80 min, and 1,000 min. A set of 15 flasks (each of three flasks for each of the given contact time) without adding mycomass were utilized as control. All flasks were placed on a rotator shaker at 150 rpm. After 20 min, a set of three flasks were removed as subset A_1 to which the suspension was filtered through Whatman filter paper separating the DAFM loaded with Zn^{2+} ions. The amount of unadsorbed Zn^{2+} (remaining the solution after biosorption) was recorded on an AA-7000 model AAS in the Department of Botany, Chaudhary Charan Singh University, Meerut (Uttar Pradesh, India). Similarly, each of the subsets of three flasks (A_2, A_3, A_4, and A_5) was removed after 40, 60, 80, and 100 min. The procedure for all subsets was repeated after 20 min. Another set of three flasks filled with 100 mL of 100 ppm zinc solution, without DAFM, served as control. The efficiency of DAFM in all flasks was assessed and analyzed as those for the effect of DAFM age and particle size. Similarly, five sets were used for the optimization of temperature, DAFM dose, and initial zinc concentration. To these sets, the experiments and procedures were as follows:

(i) 15 flasks for temperature variable (three for 25 °C, three for 35 ºC, three for 45 °C, three for 55 °C, and three for 65 °C);

(ii) 15 flasks for DAFM dose variable (three for 10 mg, three for 20 mg, three for 30 mg, three for 40 mg, and three for 50 mg mycomass dose); and

(iii) 15 flasks for initial zinc concentrations (three for 100 ppm, three for 200 ppm, three for 300 ppm, three for 400 ppm, and three for 500 ppm).

A set of five flasks filled with 100 mL of 100 ppm zinc solution, without DAFM, served as control for the temperature variable. Another set of five flasks filled with similar content, without adding DAFM, served as the control for the DAFM dose variable. One more set of five flasks filled with different concentrations of zinc (100, 200, 300, 400, and 500 ppm), without adding DAFM, served as the control for initial Zn^{2+} concentrations. The efficiency of DAFM to all these flasks was evaluated and assessed as those for contact time variable. The Fourier-transform infrared (FT-IR) spectroscopy of DAFM before (unloaded), and after (Zn-loaded) biosorption was carried out for the confirmation of DAFM surface functional sites involved in Zn^{2+} biosorption. Before analysis, the samples of DAFM were dried for 24 h at 80 °C. For FTIR analysis, KBr pellets were prepared containing 1.5 mg of the DAFM sample adding 200 mg of KBr. The spectra were recorded on an IR Affinity-1 SHIMADZU spectrophotometer, Sr. no. A21374801220 (at CCS University Meerut, Uttar Pradesh, India) in the range of 4,000 to 500 cm^{-1}.

Calculation of specific Zn^{2+} uptake by DAFM

The specific amount of Zn^{2+} taken up by DAFM was calculated using the following equation:

$$qe = \frac{V\left(C_i - C_f\right)}{W} \quad (1)$$

The adsorption percentage was determined using the following formula:

$$\%\ Biosorption = \frac{(C_i - C_f)}{C_i} \times 100 \quad (2)$$

where, q_e represents the quantity of adsorbed Zn^{2+} ($mg{\cdot}g^{-1}$ mycomass); V is the volume of aqueous zinc solution (L); C_i is initial Zn^{2+} concentration in aqueous solution (ppm); C_f is the final concentration of zinc solution after biosorption (ppm); W is the added DAFM dose (dry weight in g).

Isotherm models used for the study of Zn^{2+} biosorption onto DAFM

For the analysis of adsorption equilibrium data, three widely applicable isotherm models were used such as Langmuir[43], Freundlich[44], and Tempkin[45]. These models were applied for single solute systems to depict the adsorption equilibria of the DAFM and represented by the following equations:

Langmuir's model:

$$\frac{C_e}{q_e} = \frac{1}{K_L q_{max}} + C_e/q_{max} \quad (3)$$

Freundlich's model:

$$Logq_e = LogK_F + \frac{1}{n}LogC_e \quad (4)$$

Tempkin's model:

$$q_e = B_T LnK_T + B_T LnC_e \quad (5)$$

where, q_e ($mg{\cdot}g^{-1}$) for all the three isotherm models indicates the adsorbed amount of adsorbate per unit mass of adsorbent at equilibrium; q_{max} ($mg{\cdot}g^{-1}$) is characteristic feature of Langmuir's model which represent the maximum (monolayered) adsorption capacity of adsorbent to its per unit weight; K_L ($L{\cdot}mg^{-1}$) is a constant of Langmuir's model which is directly associated to the affinity of functional sites to the pollutant (Zn^{2+}); C_e ($mg{\cdot}L^{-1}$) reflects the equilibrium metal concentration; K_F is one of the Freundlich's constants which determines whether the conditions are favorable for biosorption and thus, depicts the influence of adsorption process on adsorption capacity; and $1/n$ reflects one of the impactful constants of Freundlich's model which determines the effect of pollutant concentration on adsorption capacity and thus indicates the intensity of adsorption.

Herein, the determination of some other characteristic constants such as B_T ($RT{\cdot}b^{-1}$) and K_T ($L{\cdot}mg^{-1}$) of Tempkin's model can not be denied. B_T reflects the heat of adsorption, whereas K_T is a constant representing the binding of pollutant to the adsorbent at equilibrium, and corresponds to the maximum energy of the binding process. b ($J{\cdot}mol^{-1}$) is another constant of Tempkin's model; R (8.314 $J{\cdot}K^{-1}{\cdot}mol^{-1}$) is universal gas constant; and T is the temperature in celsius[42,46].

Kinetic study of Zn^{2+} biosorption onto DAFM

To interpret the mechanism of adsorption, at pH = 7.0, 100 mL of 50 ppm zinc solution was taken into a set of 27 flasks at 25 °C temperature and 10 mg dose of DAFM was added to these flasks. All these flasks were stirred well at 150 rpm. The sets of three flasks each were removed at intervals of 10 min, until 90 min of the final set. The suspension was filtered and examined for residual Zn^{2+} concentration through AAS. These findings were proved using contact time studied for interpretation of biosorption kinetics and measurement of residual Zn^{2+} concentration at equilibrium[20,47]. The adsorption kinetics were investigated via two kinetic models, i.e., pseudo-first order (PFO) and pseudo-second order (PSO) as mentioned in Eqs (6) and (7). These models can be expressed using the following equations:

PFO model:

$$Log\,(q_e - q_t) = LogInq_e - K_1 t \quad (6)$$

PSO model:

$$\frac{1}{q_e} = \frac{1}{K_2 q_e^2} + \frac{1}{q_e}t \quad (7)$$

where, q_e is the amount of Zn^{2+} adsorbed per unit weight of DAFM ($mg{\cdot}g^{-1}$) at equilibrium; qt ($mg{\cdot}g^{-1}$) denoted to the amount of Zn^{2+} adsorbed per unit weight of DAFM at different 't'; K_1 (min^{-1}) and K_2 ($g{\cdot}mg^{-1}{\cdot}min^{-1}$) are the characteristic rate constants of PFO and PSO models, respectively. The value of first order rate constant (K_1) was derived from the calculations using intercept and slope of graph of $ln\,(q_e - q_t)$ vs 't' (Fig. 1a). Similarly, the value of second order rate constant K_2 was achieved by using intercept and slope of the graph of t/q_t vs 't' (Fig. 1b)[20,47].

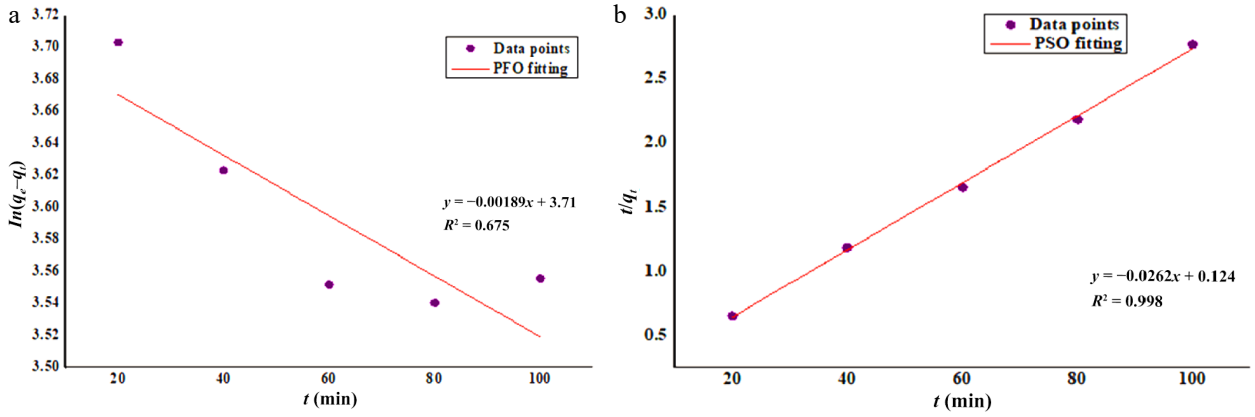

Fig. 1 Kinetics study of Zn^{2+} biosorption onto DAFM (a) PFO and (b) PSO.

Thermodynamic study of Zn^{2+} biosorption using DAFM

Thermodynamic study reveals the chemical or physical behavior of adsorption mechanism, hence the adsorption data, derived at different temperatures from 298.15 to 348.15 K, was also assessed through thermodynamic investigation. The calculations for the thermodynamic parameters ΔG^o (Gibbs free energy), ΔH^o (standard enthalpy), and ΔS^o (change in entropy) was carried out using the following equations[48]:

$$\Delta G^o = -RTInK_C \quad (8)$$

$$\Delta G^o = \Delta H^o - T\Delta S^o \quad (9)$$

where, R is the universal gas constant ($J{\cdot}mol^{-1}{\cdot}K^{-1}$); T is the indicative of temperature (K); and K_C (q_e/C_e) represents the equilibrium constant of the mechanism [Eqs (8) and (9)]. The values of ΔH^o and ΔS^o were obtained using the values of intercept and slope derived from the graphs (Fig. 2) constructed between lnK_C vs $1/T$ (K)[48].

Herein, it is also necessary to consider that thermodynamic conditions should be the same (i.e., fixed temperature and pressure) across a system, but in the case of the present investigation, the experiments for Zn^{2+} biosorption were conducted at different temperatures, i.e., non-standard conditions as well as the pressure were not the parameters studied. Therefore, the thermodynamic parameters [Eq. (9)] might be affected with the change in system environment[47] and hence, can be represented with their signs of activations [Eq. (10)]:

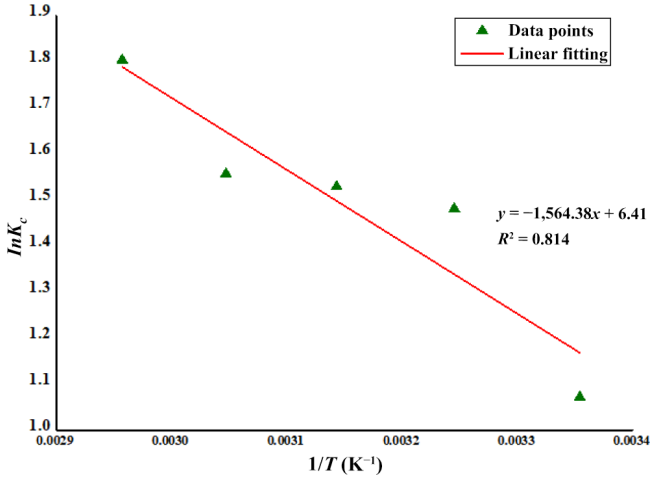

Fig. 2 Thermodynamic study of Zn^{2+} biosorption using DAFM.

$$\Delta G^{\pm} = \Delta H^{\pm} - T\Delta S^{\pm} \quad (10)$$

Using Eq. (9) another equation can also be derived in the form of Eq. (11) as:

$$InK_C = \left(\frac{\Delta S^o}{R}\right) - \left(\frac{\Delta H^o}{RT}\right) \quad (11)$$

In the same way, Eq. (10) can be re-written in the form of Eq. (12) as:

$$InK_C = \left(\frac{\Delta S^{\pm}}{R}\right) - \left(\frac{\Delta H^{\pm}}{R}\right) \quad (12)$$

Change in standard enthalpy ($\Delta H^{\pm}$) was represented with its sign of activation. Similarly, the change in entropy was also represented with its activation sign ($\Delta S^{\pm}$). Both $\Delta H^{\pm}$ and $\Delta S^{\pm}$ were obtained using Eq. (12) and verified with the calculations using intercept and slope of the graph constructed between lnK_C vs $1/T$ (K) (Fig. 2).

Results and discussion

Optimization of parameters for Zn^{2+} biosorption onto DAFM

Removal of a given pollutant from aquatic solution using a specific adsorbent might have optimal conditions for maximum results. This approach can be assigned to the reason that, the efficiency of any adsorbent might vary with different adsorbates also affected by the system conditions. Thus, it is necessary to investigate the optimal conditions for an adsorbent to be used effectively and economically. Several studies are available suggesting the effects of contact time, temperature, pH, adsorbent amount, and adsorbate concentration etc. on the biosorption of metals/dyes. Keeping in mind the recent findings, the present investigation was focused on the biosorption of Zn^{2+} by DAFM as well as the optimization of DAFM age, DAFM particle size, contact time, temperature, DAFM dose, and initial Zn^{2+} concentration for effective biosorption.

Effect of DAFM age and particle size on biosorption of Zn^{2+}

The age and particle size of mycomass particles are crucial features that influence their properties to interact with surrounding pollutant/metal ions in a biosorption process. After the optimization of these two factors, the effective removal of pollutants could be achieved. In this respect, the present study was conducted to adsorb Zn^{2+} from its aqueous solution using DAFM of different ages (48, 96, and 144 h) and particle size (355–500, 250–355, and 125–250 μm) at 25 °C, pH = 7.0, from 50 $mg{\cdot}L^{-1}$ $ZnSO_4$ solution. Figure 3 represents the effect of the age of DAFM and its particle size on biosorption of Zn^{2+} from its 50 ppm aqueous solution.

Among the mycomass ages, the adsorption capacity of 48 h old DAFM was always lower than those of 96 and 144 h old DAFM (Fig. 3). However, the adsorption capacity of 96 h old DAFM was higher in comparison of other mycomass ages, but the marked difference between 96 and 144 h old DAFM was very little, and thus, could be ignored. At a look at the effect of particle size, the trend was similar that the adsorption capacity of 96 h old mycomass was always higher than those of 48 and 144 h old mycomass with different particle size studied. Thus, concluding from Fig. 3, the maximum adsorption capacity (q_e = 28.54 mg·g^{-1}) was obtained with 96 h old mycomass with its 125–250 μm particle size. The performance of 96 h old DAFM could be ascribed as the older mycelium (over 96 h of age) becomes comparatively highly vacuolated than those of younger. With growing age, the fungal mycelium goes to dying and decaying through developing hyphal aggregations[49] as well as distortion of functional groups resulting in decreased capability to adsorb pollutants like metals. The mycomass of younger age was found to have excellent capacity to adsorb the metal in comparison to that of the older ones. Similar effects of mycomass age were investigated by other workers using different mycomass for biosorption of metals[36,50,51].

Figure 3 also depicts the effect of particle size of mycomass on adsorption capacity of DAFM to adsorb Zn^{2+}. The adsorption capacity (q_e) was increased from 12.42 to 24.62 mg·g^{-1} with decreasing particle size from 500–355 to 250–125 μm with 48 h old DAFM. With 96 h old mycomass, the adsorption capacity was increased from 23.48 to 28.54 mg·g^{-1} at change of particle size from 500–355 to 250–125 μm. The adsorption capacity with 144 h old DAFM was slightly lower than those of 96 h old DAFM, but it was higher than those of 48 h old DAFM. Thus, it is clear that the mycomass of bigger particle size (i.e., 355–500 μm) has yielded the lower removal with all the mycomass ages. On the other hand, the mycomass of comparatively smallest particle size (i.e., 125–250 μm) has yielded the maximum adsorption of Zn^{2+} ions. The increased adsorption capacity using DAFM of smaller particle size could be due to the increase in total surface area of mycomass which probably has made more adsorption sites available for maximum binding of metals. Additionally, the smaller size of mycomass allowed a quicker uptake of metal ions through the interactions followed by bond formation between metal ions and adsorption sites of the DAFM surface[52]. Moreover, considering the effect of age, the DAFM has yielded the maximum removal of metal with the combination of 96 h age and 125–250 μm particle size. The investigated particle sizes of DAFM under entire

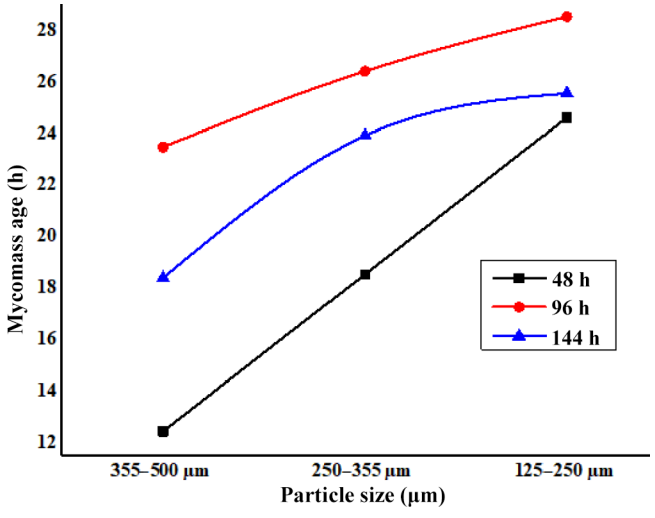

Fig. 3 Effect of age and particle size of DAFM on biosorption of Zn^{2+}.

mycomass ages revealed that, the performance of smallest particle size (125–250 μm in this work) was excellent at the biosorption of Zn^{2+} (Fig. 3). Therefore, in the present work, the mycomass of 96 h age and 125–250 μm particle size was selected for further studies on the biosorption of Zn^{2+} using DAFM.

Effect of contact time on Zn^{2+} biosorption

The duration of contact between biomass and adsorbate is also a key factor that affects their interaction and consequent binding. Optimization of contact time is thus, essential for achieving maximum results. Therefore, the present study was conducted working on biosorption of Zn^{2+} at different contact times (20 to 100 min at a regular interval of 20 min) between Zn^{2+} ions and DAFM particles in 100 ppm Zn^{2+} solution using 10 mg/100 mL doses of optimized DAFM age (96 h) and particle size (125–250 μm); and the temperature was kept the same (25 °C) as previous experiments. Figure 4a represents the effect of contact time on the biosorption of Zn^{2+} onto DAFM in the form of adsorption capacity and percent biosorption. The adsorption capacity went from ascending with increasing contact time from 10 min to 80 min, which later decreased when the contact time was elevated to 100 min. The increased uptake of Zn^{2+} on DAFM (36.56 mg·g^{-1}) along with the highest adsorption percentage (86.55%) was achieved and equilibrium was practically attained at 80 min contact time. The increased adsorption at longer contact time is likely because the longer contact time allows the facilitation of more functional sites to be active for more binding of Zn^{2+} ions as reported by recent researchers[46,53]. However, the adsorption capacity was decreased at higher contact times (after 80 min); the concentration of Zn^{2+} metal ions was not so high which could be attributed either to: (i) the cohering/blending of DAFM particles[46] causing the blockage of functional adsorption sites making those unavailable for Zn-binding; or (ii) the saturation of all the free binding sites on DAFM resulting in single layer (on outer surface) adsorption of Zn^{2+}[36].

Impact of temperature on Zn^{2+} removal

Temperature is also a parameter that can not be ignored in the determination of adsorption capacity of any adsorbent. In any adsorption-based water-treatment system, an optimal thermal condition is an intense requirement for achieving the maximum results. It influenced the adsorption phenomena due to its effect on mycomass-metal binding complexes through the ionization of cell wall components[53]. Therefore, for the removal of Zn^{2+} through biosorption using DAFM, the present research was conducted at a wide range of temperatures, viz., 25, 35, 45, 55, and 65 °C (Fig. 4b). During the study of thermal effect, it was observed that the adsorption capacity was increased from 36.56 to 42.94 mg·g^{-1} on increasing temperature from 25 to 65 °C, hence, the maximum removal was found at 65 °C. The increase in adsorption capacity at each level of increased temperatures can be ascribed to the reason that the temperature provides the required energy which induce the breakdown of certain chemical barriers, thus facilitating the binding of metal ions onto biosorbent surface[54]. Therefore, 65 °C was considered as one of the components of optimal temperature for this study.

Effect of DAFM concentration

Figure 4c delineates the effect of mycomass amount on DAFM's equilibrium on Zn^{2+} uptake from 100 ppm $ZnSO_4$ solution at optimized contact time and temperature. Different dosages of DAFM were tried such as 10, 20, 30, 40, and 50 mg. The maximum Zn^{2+} ions removal was recorded with 30 mg/100 mL DAFM dose. Further increase in DAFM dose has resulted in decreased percentage as well as adsorption capacity. The maximum percent removal of Zn^{2+} was 96.92% with adsorption capacity q_e = 15.64 mg·g^{-1}. Decrease in

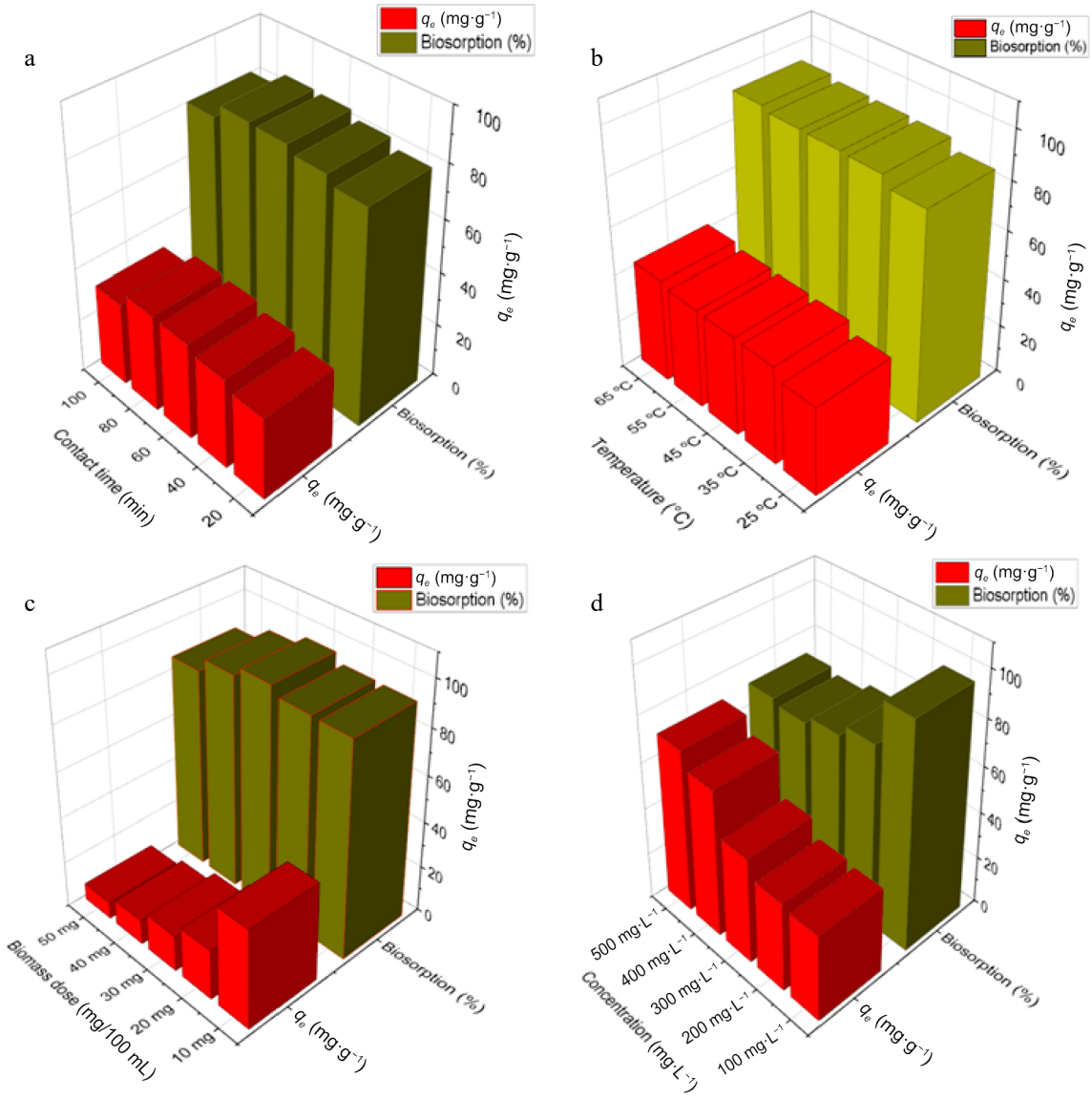

Fig. 4 Effect of different parameters on biosorption of Zn^{2+} by DAFM. (a) Effect of contact time; (b) effect of temperature; (c) effect of DAFM dose; and (d) effect of initial Zn^{2+} concentrations.

adsorption percentage at the DAFM dose beyond 30 mg/100 mL can be attributed to higher density of adsorption sites interfering with one another resulting in a gradual decline in percent removal. It can be the result of reduction in the ration of interfering metal ions with mycomass particles.

Effect of initial strength of Zn^{2+} ions on the adsorption capacity of DAFM

The strength of metal ions can alter the metal removal efficiency through a set of factors such as the availability of specific surface functional groups and the ability of surface functional groups to bind metal ions. Initial concentration of solution can provide an important driving force to overcome the mass transfer resistance of metal between the aqueous and solid phases. The biosorption of Zn^{2+} onto the DAFM surface was found decreasing with increasing Zn^{2+} ion concentrations under study. Figure 4d delineates that the maximum percentage removal (96.92%) was attained at 100 ppm Zn^{2+} concentration while the maximum adsorption capacity was achieved at 500 ppm Zn^{2+} concentration. With the increased concentration of Zn^{2+} metal ions, its adsorption increased. The maximum removal 71.04% of 500 mg·L^{-1} of Zn^{2+} was obtained after 80 min of contact period while removing 96.92%, 77.82%, 72.59%, and 68.96% respectively for 100, 200, 300, and 400 ppm. The adsorption percentage moved from a successive decline upto the 400 ppm zinc concentration which further increased a little at 500 ppm, as such, the adsorption capacity was highest at 500 ppm Zn^{2+} concentration which was calculated as q_e = 70.13 mg·g^{-1}. The decreasing trend of percent removal with elevating metal concentration can be ascribed due to one of the reasons either: (i) at lower metal concentrations, the metal ions in the aqueous medium would interact with the binding sites of DAFM and left unadsorbed in the solution due to the electrostatic repulsion and/or saturation of binding sites as reported by Jalija et al.[55] and Ong et al.[56]; or (ii) at higher concentrations the number of empty functional sites decreased, thereby tending to decrease in adsorption percentage. Contrary to this, increasing the adsorption percent beyond 400 ppm Zn^{2+} concentration might be caused by the agglomeration of metal ions due to increased driving forces to overcome all mass transfer resistance of metal ions between liquid and solid phase, resulting in maximum chances of collision between metal ions and mycomass[57,58].

Isothermic evaluation of biosorption of Zn^{2+} onto DAFM

For accurate analysis of adsorption capacity and equilibrium behavior of DAFM[50], the adsorption data was examined with three of the universal isotherm models, viz., Langmuir[43], Freundlich[44], and Tempkin[45] isotherm models. The isotherm models are mathematically utilized to describe the relationship between the concentration of solute in the aqueous solution and the amount of solute adsorbed onto solid surface of the mycomass. For the investigation of isotherm, the adsorption data was analysed at different metal concentrations such as 100, 200, 300, 400, and 500 ppm.

LIM

For its reliability and versatility, the Langmuir isotherm model is widely applied in adsorption studies. It represents the homogenous sorption mechanism and relied on the concept of monolayer adsorption. According to Langmuir's model the force between adsorbed ions are not significant and that a limited number of active sites are present on the adsorbent's surface. Therefore states that, once metal ions adsorbed at adsorbent's surface, these occupy the functional sites and hence, no further adsorption occur. Figure 5a represents the graph plotted C_e/q_e vs C_e at varied metal concentrations. At 500 ppm initial Zn^{2+} concentration, the maximum adsorption capacity (q_{max}) of DAFM was 65.79 mg·g^{-1} with correlation coefficient R^2 = 0.929, which suggests the monolayer adsorption of zinc metal forming a complete single layer of metal on DAFM surface. The maximum adsorbed capacity (q_{max} = 65.79 mg·g^{-1}) of the metal is close to the value obtained experimentally (q_e = 70.13 mg·g^{-1}) and thus, it is comparable indicating the fitness of the model to the experimental data. The binding affinity constant of Langmuir's model (K_L = 0.051 L·mg^{-1}) was calculated using the intercept of the graph (Fig. 5a and Table 2) which indicated a higher affinity of metal ions toward the adsorption sites of DAFM[59–61]. The adsorption of Zn^{2+} onto DAFM was chemisorption, as indicated by q_{max} and K_L.

FIM

The empirical form of Freundlich's equation relies on multilayer formation of adsorbate on the heterogeneous surfaces of biosorbents in which the biosorbent surface is enriched with heterogeneously dense functional sites. The parameters calculated for Freundlich's model by employing its linear form are given in Table 2 and Fig. 5b. Freundlich isotherm parameters were calculated using the intercepts and slope of the plot between *log qe* and log *Ce*. For the Freundlich's isotherm model, the adsorption is considered promising if value of K_F is found in range of 1–20[62], but the results reveal in the present research that, K_F was 196.47 mg·L^{-1} for linearity of the model which indicated that the biosorbent is highly capable of removing Zn^{2+} ions from aqueous solution as also the process is physisorption[63]. The adsorption intensity represented by 1/*n* indicates fitness of this model for biosorption if value of 1/*n* is in the range of 0 to 1, which in the present study was beyond the unity (1/*n* = 2.68) indicating the high suitability of DAFM for Zn^{2+} removal under studied conditions[64] as well as the unfavorable and irreversible process. This value of 1/*n* (2.68) also indicated stronger interaction between the adsorbent and the adsorbate and the adsorption capacity is only slightly suppressed at lower equilibrium concentrations[64,65]. The value of R^2 (0.966) obtained from the plot is significant, representing good fitness as well as the best fitting of this model for biosorption of Zn^{2+} onto DAFM over other isotherm models under study.

TIM

Tempkin isotherm determines the heat of the sorption process and thus utilized to understand the mechanism of adsorption. This model helps in the prediction that the equal distribution of binding energies tied to surface adsorption, therefore, provides accurate knowledge about the process. It is based on the assumption that, the decline in heat related to the biosorption, increases linearly with increasing coverage of adsorbent's surface. A plot of q_e vs log C_e (Fig. 5c and Table 2) delineates the determination of isotherm constants B_T and K_T calculated from the slope and intercept of the graph, respectively. The equilibrium binding constant (K_T) represents the maximum binding energy of the process, and the other constant B_T represents heat of the particular adsorption experiment[66]. Figure 5c suggests that the linearity of the Tempkin model was not found to be suitable with a positive value of the binding energy constant (K_T = 2.0 L·mg^{-1}). The magnitude of B_T (9.55 J·mol^{-1}) indicated the process as chemisorption. The correlation coefficient (R^2 = 0.861) generated by the plot (Fig. 5c) and the Tempkin equilibrium constants indicated that this model does not satisfy the experimental data[67].

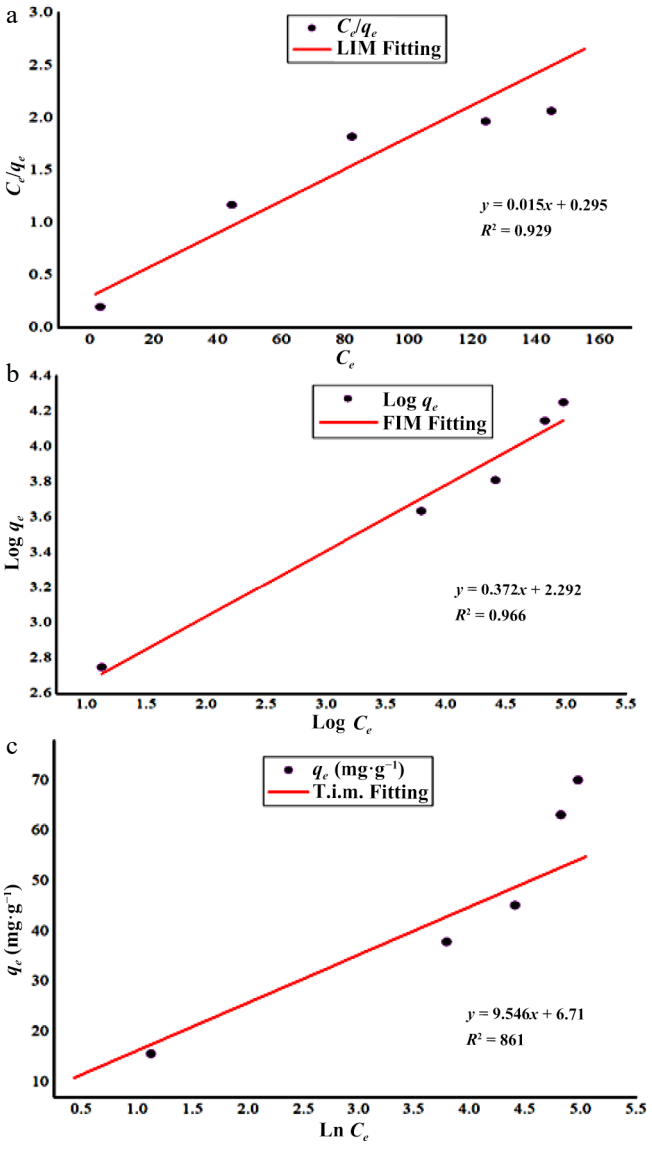

Fig. 5 Isothermic study of Zn^{2+} biosorption onto DAFM. (a) Langmuir's isotherm; (b) Freundlich's isotherm; and (c) Tempkin's isotherm.

Table 2 represents the model fitness which provides the comparison based on correlation coefficient values along with the constants for each isotherm model. As a perusal of the graphical representation of each of the used isotherm models (Fig. 5a–c), the Freundlich model with a maximum value of correlation coefficient (R^2 = 0.966) best describes the removal of Zn^{2+} ions. Besides this, the adsorption intensity is less than unity ($1/n$ = 0.37), suggesting the favorability of the process[67,68]. The maximum adsorption capacity obtained by Freundlich's model (q_{max} = 65.79 mg·g^{-1}) is close to the adsorption capacity calculated from experimental data (q_e = 70.13 mg·g^{-1}). On the other hand, the value of the high affinity constant (K_F = 196.47 L·mg^{-1}) indicated the favorability of DAFM to remove Zn^{2+} ions and suggested the process is a physical adsorption.

Kinetic interpretation of biosorption of Zn^{2+} onto DAFM

Predicting the dynamics of the adsorption mechanism and understanding the factors governing the rate of the adsorption process needs to employ kinetic study, especially the utilization of PFO and PSO models to the biosorption data. Kinetic study also determines whether the process is a physisorption or chemisorption to which the authentication derived from comparison of correlation coefficients, since the authenticity and reliability of the biosorption mechanism for both the kinetic models is expressed in the form of values of correlation coefficients (R^2). In Fig. 1 and from Eq. (6), the slope of the graph T (time) vs $ln(q_e–q_t)$ suggests the rate limiting constant (K_1) and the intercept gives the adsorption capacity ($q_{e\ (cal.)}$, mg·g^{-1}). From Fig. 1a, b and Table 3, it is clear that, the value of correlation coefficient of PSO is higher (R^2 = 0.998) in comparison of PFO (R^2 = −0.238) indicated the adsorption rate-limiting step of the process is a chemical interaction accomplished between functional sites of DAFM and Zn^{2+} ions. Also, the value of the correlation coefficient of PFO is comparatively very low, indicating that the rate-limiting step in the biosorption process was purely through the chemical interactions instead of the physical process[69]. It was also found that the derived value of K_2 (0.01 g·mg^{-1}·min^{-1}) was higher than that of K_1 (1.89×10^{-5} g·mg^{-1}·min^{-1}) which also gives the confirmation about chemisorption process. This mechanism behavior indicated that the retention of Zn^{2+} ions onto the DAFM surface was through two successive seminal stages: (i) first step involve the binding of Zn^{2+} ions to the primarily exposed functional sites of DAFM due to their maximum chances to join each other; and (ii) the retention of Zn^{2+} ions can be due to the stabilization of the complex formed in the first step takes place through the chemical bonds with another superficial groups[70]. Based on the calculations of these two parameters, it can be attributed that the main rate-limiting step is the chemical adsorption. The PFO does not fit the adsorption data as observed from the correlation coefficient and rate-limiting component, while the PSO fits well to the adsorption data which suggests that the solute transfer is accomplished by mass transfer, which might be followed by surface adsorption, external diffusion, and/or intra-particle diffusion[71–74].

Table 2. The values of parameters of different isotherm models studied for biosorption of Zn^{2+} onto DAFM.

LIM	FIM	TIM
$q_{e\ (exp.)}$ (mg·g^{-1}) = 70.13		
q_{max} (mg·g^{-1}) = 65.79	K_F (L·mg^{-1}) = 196.47	B_T (J·mol^{-1}) = 9.55
K_L (L·mg^{-1}) = 0.51	$1/n$ = 0.37	K_T (L·mg^{-1}) = 2.0
R^2 = 0.929	R^2 = 0.966	R^2 = 0.861

Table 3. Values of kinetic parameters for biosorption of Zn^{2+} onto DAFM.

PFO	PSO
$q_{e\ (exp.)}$ (mg·g^{-1}) = 70.13	
$q_{e\ (cal.)}$ (mg·g^{-1}) = 42.52	$q_{e\ (cal.)}$ (mg·g^{-1}) = 38.21
K_1 (g·mg^{-1}·min^{-1}) = 1.89×10^{-5}	K_2 (g·mg^{-1}·min^{-1}) = 0.01
R^2 = 0.675	R^2 = 0.998

Thermodynamic evaluation of biosorption of Zn^{2+} ions onto DAFM

The analysis of thermodynamic parameters, which include the change in biosorption enthalpy ($\Delta H^{\ddagger}$), Gibbs free energy ($\Delta G^{\ddagger}$), and entropy (($\Delta S^{\ddagger}$), has been investigated at different temperatures. The values of $\Delta H^{\ddagger}$ and $\Delta S^{\ddagger}$ were calculated using intercept and slope of the graph of lnK_C vs $1/T$ (Fig. 2). Increased value of $\Delta H^{\ddagger}$ indicates the temperature assisted process and can be further induced by rising temperature. Contrary to this, a negative value of $\Delta G^{\ddagger}$ could be ascribed that the adsorption mechanism is spontaneous and its magnitude increases proportionally with the rise in temperature[75]. Some of the studies explored have opined that these parameters are relatively beyond the dependency of temperature and hence, can be considered with reliable accuracy. A study conducted by Ortiz-Oliveros et al.[76] has suggested the slight dependency of these two parameters to temperature. This has led to the proposal of thermodynamic relationship between $\Delta H^{\ddagger}$ and $\Delta S^{\ddagger}$.

For the present investigation the magnitude of thermodynamic parameters enthalpy ($\Delta H^{\ddagger}$), Gibbs free energy ($\Delta G^{\ddagger}$) and entropy ($\Delta S^{\ddagger}$) are given in Table 4. The table demonstrates that the values of free energy were negatively increasing with increasing temperatures (from −15.88 to −18.01 kJ·mol^{-1}) for the biosorption of Zn^{2+} ions onto DAFM, which indicates the spontaneity of the adsorption mechanism that was proportional to temperature[65]. It also enlightens the opinion that more functional groups on DAFM surface became activated at elevating temperatures, allowing the energy barrier to overcome the hindrance[77,78]. The magnitude of entropy ($\Delta S^{\ddagger}$= 53.29 J·K^{-1}·mol^{-1}) is higher than the enthalpy ($\Delta H^{\ddagger}$= 13.01 kJ·mol^{-1}), and the higher magnitude of entropy change can be attributed to the increased degree of freedom of the released metal ions during the exchange of ions originating from the DAFM surface[79]. These findings also indicate an increased randomness at the solid-liquid interface for the adsorption of metal ions onto DAFM caused by the higher affinity of the adsorbent towards Zn^{2+} ions. Also the positive magnitude of change in enthalpy ($\Delta H^{\ddagger}$= 13.01 kJ·mol^{-1}) indicate the endothermic adsorption of Zn^{2+} onto DAFM. Similar findings were found in an another study of Cu(II) biosorption using biochar derived from algal biomass, the calculated parameters gave the affirmation of a spontaneous and feasible process[78]. Concluding the magnitudes of calculated thermodynamic parameters it is feasible to say that the biosorption of Zn^{2+} ions onto DAFM is endothermic, spontaneous and more favorable at high temperature[79].

Table 4. Calculated thermodynamic parameters for Zn^{2+} biosorption onto DAFM.

Adsorbent	T (K)	$\Delta G^{\ddagger}$ (kJ·mol^{-1})	$\Delta H^{\ddagger}$ (kJ·mol^{-1})	$\Delta S^{\ddagger}$ (J·K^{-1}·mol^{-1})	Correlation coefficient
DAFM	298.15	−15.88	13.01	53.29	R^2 = 0.814
	308.15	−16.41			
	318.15	−16.94			
	328.15	−17.48			
	338.15	−18.01			

Some recent studies indicating the biosorption potential of different adsorbent materials (of biological or non-biological origin) for the biosorption of Zn^{2+} are summarized below in Table 5. The table gives a comparative view of those adsorbents with the present investigation suggesting the usability of DAFM for the removal of Zn^{2+} over other adsorbents.

FT-IR analysis of DAFM before and after Zn^{2+} removal

The DAFM was examined before and after the biosorption of Zn^{2+} and the functional groups of mycomass responsible for removal of metal were identified with IR Afnity-1 Shimadzu spectroscopy at the Department of Botany, Choudhary Charan Singh University, Meerut, Uttar Pradesh, India. It is visible from Fig. 6 and Table 6 that there were many functional groups involved in the biosorption of Zn^{2+}. Before biosorption (Fig. 6a) of metal, the mycomass surface was found to have 13 sharp peaks containing 45 functional groups of 25 types. The peaks contain different functional groups as follows: C-CH_3 (1:1385.5), aromatic azo (1:1385.5 and 1:1419.6), sulphate (1:1385.5), alcohol (1:1385.5), sulfonyl chloride (1:1385.5), phenol (1:1385.5), CH_2 (1:1419.6), CH_3 (1:1419.6), carboxylic acid (1:1419.6, 1:1683.8, 1:1716.6, and 1:1734), aromatic ring (1:1456.2 and 1:1508.3), alkane (1:1456.2), nitro (1:1508.3, 1:1541.9, 1:1558.4, and 1:1575.8), aliphatic azo (1:1541.9, 1:1558.4, and 1:1575.8), aromatic/hetero ring (1:1558.4 and 1:1575.8), amide (1:1558.4, 1:1575.8, 1:1647.2, and 1:1683.8), alkene (1:1647.2), ketone (1:1647.2 and 1:1683.8), C=C (1:1647.2), C=N (1:1647.2), imine (1:1683.8), urethane (1:1716.6), aldehyde (1:1716.6 and 1:1734), ester (1:1716.6 and 1:1734), aliphatic ester (1:2341.5), and pH (1:2341.5 and 1:2360.8).

After biosorption of Zn^{2+} the number of sharp peaks was reduced to 6. The visible peaks were laden with 22 functional groups of 18 types, showing the involvement of 22 functional groups in the biosorption of the metal. Visible peaks after biosorption (Fig. 6b) contain functional groups as follows: C-CH_3 (1:1373.3), aromatic azo (1:1373.3), alcohol (1:1373.3), phenol (1:1373.3), carboxylic acid (1:1373.3, 1:1651, and 1:1732), aromatic ring (1:1456.2), nitro (1:1539.1 and 1:1556.5), aliphatic azo (1:1556.5), aromatic/hetero ring (1:1556.5), amide (1:1556.5 and 1:1651), ketone (1:1651), C=C (1:1651), C=N (1:1651), imine (1:1651), alkene (1:1651), ester (1:1732), aliphatic ester (1:1732), and aldehyde (1:1732).

The aforementioned data reflects the involvement of 20 functional groups of 15 types. Of those, nine groups of seven types such as – aromatic azo (1), sulphate (1), sulfonyl chloride (1), nitro (1), aliphatic azo (2), aromatic/hetero rings (1) and amide (2) were identified as strong binders, and eight functional groups of seven types including carboxylic acid (2), aromatic ring (1), nitro (1), ketone (1), urethane (1), aldehyde (1) and ester (1) – were moderate binders. Besides those two groups i.e., C–CH_3 and P–H were found to make weak bonds with Zn^{2+} ions.

The reduced number of sharp peaks is the indication of the vanishing of seven peaks and thus, confirmed the involvement of their functional groups in the removal of metal. On the other hand, the shift of peaks from 1,385.5 to 1,373.3 cm^{-1} showed the involvement of S=O stretch and was attributed to the C=O bending vibration of carboxyl group; from 1,541.9 to 1,539.1 cm^{-1} of N=N stretching of proteins; from 155.4 to 1,556.5 cm^{-1} of N–O stretch and N–H bend; from 1,647.2 to 1,651 cm^{-1} of N–H bend of amine group and C=O stretch[81,93], and 1,734 to 1,732 cm^{-1} C=O stretch[94,95]. Besides those, the vanished peaks such as 1,419.6, 1,508.3, 1,575.8, 1,683.8, 1,716.6, 2,341.5, and 2,360.8 cm^{-1} have confirmed the involvement of S=O stretch, C–C stretch, N–O stretch, N–H bend[47], N=N stretch, C=O stretch, C–H bend, and stretching vibrations. Such kind of characteristic can be ascribed due to the result of alignment Zn^{2+} ions with active functional sites of DAFM which caused the change in vibration frequency. The functional groups underneath the wavelengths of vanished peaks as well as the groups of altered peaks, were assumed to be actively participating in the removal of metal

Table 5. Comparable potential of some adsorbents for Zn^{2+} biosorption in recent years.

Adsorbents	Zn^{2+} removal %/ uptake ($mg \cdot g^{-1}$)	Ref.
Graphite-iron alloy	72.5%	[79]
Penicillium sp.	52.14 $mg \cdot g^{-1}$	[80]
Aspergillus terreus	10.7 $mg \cdot g^{-1}$	[81]
Microcystis aeruginosa	67 $mg \cdot g^{-1}$	[82]
Gauva leaves	14.5 $mg \cdot g^{-1}$	[65]
Aspergillus terreus	10.7 $mg \cdot g^{-1}$	[81]
Tinospora cordifolia	87%	[83]
Agaricus biosporus biomass	19.61 $mg \cdot g^{-1}$	[84]
Inula viscosa leaves	85%	[20]
Lantana camara leaves	2.778 $mg \cdot g^{-1}$	[85]
Walnut carbon nanoparticles	90%	[86]
Sargassum myriocystum	86.67%	[87]
Spirulina platensis	50.7 $mg \cdot g^{-1}$	[78]
Reynoutria japonica	17 $mg \cdot g^{-1}$	[88]
Dalbergia sissoo sawdust	6.36 $mg \cdot g^{-1}$	[89]
Pithophora cleveana	13.58 $mg \cdot g^{-1}$	[90]
Groundnut husk ash	80.00%	[91]
Penicillium simplicissimum	1.25 $mg \cdot g^{-1}$	[92]
DAFM	70.13 $mg \cdot g^{-1}$	Present study

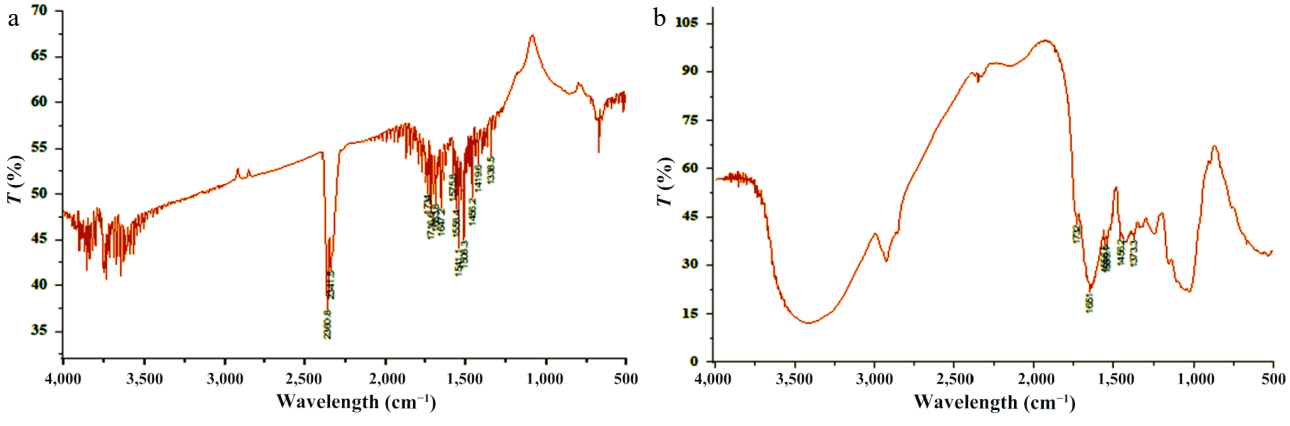

Fig. 6 FT-IR spectra of DAFM. (a) Before biosorption of Zn^{2+} and (b) after biosorption of Zn^{2+}.

Table 6. Functional groups of DAFM before and after biosorption of Zn^{2+} and the involved functions groups with relevant stretching or bending/vibrations.

Functional groups	Before biosorption	After biosorption	Functional groups involved in biosorption	Stretching/ bending/ vibration
C–CH_3	1	1	–	–
Aromatic azo	2	–	2	C–C stretch
Sulfate	1	–	1	S=O stretch
Sulfonyl chloride	1	–	1	S=O stretch
Alcohol	1	1	–	–
Phenol	1	1	–	–
CH_2	1	1	–	–
CH_3	1	–	1	C=O stretch
Carboxylic acid	5	3	2	C=O stretch
Aromatic ring	2	1	1	C–C stretch
Alkane	1	1	–	–
Nitro	4	2	2	N–O stretch
Aliphatic azo	3	1	2	N=N stretch
Aromatic/hetero rings	2	1	1	C–C stretch
Amide	4	2	2	N–H bend
Ketone	2	1	1	C–C stretch vibration
C=C	1	1	–	–
C=N	1	1	–	–
Alkene	1	1	–	–
Imine	1	1	–	–
Urethane	1	–	1	N–H stretch
Aldehyde	2	1	1	C=O stretch
Ester	2	1	1	C=O stretch
Aliphatic ester	1	1	–	–
P–H	2	–	2	C-H stretching vibration
Total	44 of 25 types	23 of 19 types	21 of 15 types	–

ions. The biosorption of metal through the chemical bonds has indicated a chemisorption process. Moreover, the positive charged metal ions might be able to bind with negatively charged functional sites present in the form of hydroxyl, carboxyl, amino, phosphate nitro, and halide groups on the DAFM surface via electrostatic forces[81,96]. Since lipid and polysaccharides contents of the fungal cell wall possess varied charged functional sites that make the feasibility of strong attraction to positively charged Zn^{2+} ions to bind with mycomass surface.

Conclusions

The present study demonstrated the significant potential of DAFM for its utilization as a sufficient myco-biosorbent for the biosorption of Zn^{2+} metal ions from aqueous solutions under specific optimized conditions. A series of various process factors such as DAFM age and particle size, contact time, temperature, DAFM dose, and initial Zn^{2+} concentration were examined and optimized for the maximum sorption capacity of this myco-biosorbent. The maximum zinc (Zn^{2+}) biosorption was achieved using fungal biomass aged 96 h, with a particle size range of 250–125 μm. This maximum uptake occurred within 80 min of contact time at a temperature of 65 °C, using a dose of 30 mg/100 mL of dried *Aspergillus flavus* biomass from a 500 ppm Zn^{2+} solution. The biosorption efficiency varied across different experimental conditions, reflecting the influence of multiple physicochemical parameters. This variation is primarily attributed to the structural and chemical properties of the fungal cell wall, which is rich in polysaccharides, proteins, and a variety of functional groups. FT-IR spectroscopy analysis of DAFM, conducted before and after biosorption, confirmed the presence of functional groups involved in binding metal ions. These groups facilitate metal ion interaction through mechanisms such as complexation and ion exchange, contributing to the overall biosorption capacity of the fungal biomass. The study of the impact of particle size on biosorption of Zn^{2+} has resulted in the foundation that it can be applicable to the industrial level. Moreover, the DAFM surface possesses a series of mechanisms including physical and chemical adsorptions, biomeneralization, and biotransformation; as also anionic functional molecules to remove the metal ions. Isothermic evaluation revealed that the Freundlich's isotherm model provided the best fit for the experimental data, suggesting a heterogeneous surface and multilayer adsorption of Zn^{2+} ions onto the DAFM. Kinetic studies were best described by the pseudo-second-order model (R^2= 0.998), implying that the rate-limiting step involved chemical interactions between the Zn^{2+} ions and the functional groups on the DAFM surface. Thermodynamic analysis indicated that the biosorption of Zn^{2+} onto DAFM was a spontaneous and endothermic process within the studied temperature range. The positive value of entropy change suggested an increased randomness at the solid-liquid interface during biosorption. These findings highlight DAFM as a promising, cost-effective, and environmentally friendly biosorbent for Zn^{2+} removal from contaminated water. The optimized conditions and the elucidated biosorption mechanisms provide valuable insights for the development of sustainable water treatment technologies. Further research could focus on the regeneration and reusability of DAFM, as well as its performance in more complex multi-metal contaminated water matrices, to enhance its practical applicability. The modifications of the *Aspergillus flavus* strain through genetic engineering for the specific industrial levels can be helpful to raise it as the most applicable myco-biosorbent for the future.

Ethical statements

Not applicable.

Author contributions

The authors confirm their contributions to the paper as follows: writing original draft, collecting relevant literature, finalization of experiments, writing-review, and editing: Kumar A, Singh R; analysis, supervision, and conceptualization: Tyagi A, Kumar P; mathematical computation and validation of equations: Kumar P. All authors reviewed the results and approved the final version of the manuscript.

Data availability

The datasets generated during and/or analyzed during the current study are available from the corresponding author on reasonable request.

Conflict of interest

The authors declare that they have no conflict of interest.

Dates

Received 30 April 2025; Revised 25 July 2025; Accepted 5 August 2025; Published online 9 September 2025

References

1. Sharma A, Patni B, Shankhdhar D, Shankhdhar SC. 2013. Zinc – an indispensable micronutrient. *Physiology and Molecular Biology of Plants* 19(1):11–20
2. Natasha N, Shahid M, Bibi I, Iqbal J, Khalid S, et al. 2022. Zinc in soil-plant-human system: a data-analysis review. *Science of The Total Environment* 808:152024
3. Kaur H, Garg N. 2021. Zinc toxicity in plants: a review. *Planta* 253:129
4. Kumar YP, King P, Prasad VSRK. 2006. Zinc biosorption on *Tectona grandis* L. f. leaves biomass: equilibrium and kinetic studies. *Chemical Engineering Journal* 124:63–70
5. Cesur H, Balkaya N. 2007. Zinc removal from aqueous solution using an industrial by-product phosphogypsum. *Chemical Engineering Journal* 131:203–8
6. Mishra V, Balomajumder C, Agarwal VK. 2010. Zn(II) ion biosorption onto surface of *Eucalyptus* leaf biomass: isotherm, kinetic, and mechanistic modeling. *CLEAN – Soil, Air, Water* 38:1062–73
7. Hussain S, Khan M, Sheikh TMM, Mumtaz MZ, Chohan TA, et al. 2022. Zinc essentiality, toxicity, and its bacterial bioremediation: a comprehensive insight. *Frontiers in Microbiology* 13:900740
8. Mishra PC, Patel RK. 2009. Removal of lead and zinc ions from water by low cost adsorbents. *Journal of Hazardous Materials* 168:319–25
9. Mohan D, Singh KP. 2002. Single- and multi-component adsorption of cadmium and zinc using activated carbon derived from bagasse – an agricultural waste. *Water Research* 36:2304–18
10. Srivastava VC, Mall ID, Mishra IM. 2007. Adsorption thermodynamics and isosteric heat of adsorption of toxic metal ions onto bagasse fly ash (BFA) and rice husk ash (RHA). *Chemical Engineering Journal* 132:267–78
11. Srivastava S, Thakur IS. 2006. Biosorption potency of *Aspergillus niger* for removal of chromium (VI). *Current Microbiology* 53:232–37
12. Naiya TK, Chowdhury P, Bhattacharya AK, Das SK. 2009. Saw dust and neem bark as low cost natural biosorbent for adsorptive removal of Zn(II) and Cd(II) ions from aqueous solutions. *Chemical Engineering Journal* 148:68–79
13. Zuhara S, McKay G. 2023. PCB-waste derived resin as a binary ion exchanger for zinc removal: isotherm modelling and adsorbent optimization. *Chemical Papers* 77:4843–57
14. Hoseinian FS, Irannajad M, Safari M. 2017. Effective factors and kinetics study of zinc ion removal from synthetic wastewater by ion flotation. *Separation Science and Technology* 52(5):892–902
15. Kashi G. 2023. Electrocoagulation/flotation process for removing copper from an aqueous environment. *Scientific Reports* 13:13334
16. Casqueira RG, Torem ML, Kohler HM. 2006. The removal of zinc from liquid streams by electroflotation. *Minerals Engineering* 19(13):1388–92
17. Hou W, Li Y, Xu S, Wang Q, Song K, et al. 2023. Removal of Zn^{2+} from glycolytic monomers of the polyethylene terephthalate based on electrodeposition. *Journal of Environmental Chemical Engineering* 11(3):110126
18. Akhtar FZ, Archana KM, Krishnaswamy VG, Rajagopal R. 2020. Remediation of heavy metals (Cr, Zn) using physical, chemical and biological methods: a novel approach. *SN Applied Sciences* 2:267
19. Honarmandrad Z, Javid N, Malakootian M. 2020. Efficiency of ozonation process with calcium peroxide in removing heavy metals (Pb, Cu, Zn, Ni, Cd) from aqueous solutions. *SN Applied Sciences* 2:703
20. Rouibah K, Ferkous H, Delimi A, Himeur T, Benamira M, et al. 2023. Biosorption of zinc (II) from synthetic wastewater by using *Inula viscosa* leaves as a low-cost biosorbent: experimental and molecular modeling studies. *Journal of Environmental Management* 326:116742
21. Thomas M, Melichová Z, Šuránek M, Kuc J, Więckol-Ryk A, et al. 2023. Removal of zinc from concentrated galvanic wastewater by sodium trithiocarbonate: process optimization and toxicity assessment. *Molecules* 28(2):546
22. Lim SS, Fontmorin JM, Pham HT, Milner E, Abdul PM, et al. 2021. Zinc removal and recovery from industrial wastewater with a microbial fuel cell: Experimental investigation and theoretical prediction. *Science of The Total Environment* 776:145934
23. Skotta A, Jmiai A, Elhayaoui W, El-Asri A, Tamimi M, et al. 2023. Suspended matter and heavy metals (Cu and Zn) removal from water by coagulation/flocculation process using a new bio-flocculant: *Lepidium sativum*. *Journal of the Taiwan Institute of Chemical Engineers* 145:104792
24. Kumar J, Joshi H, Malyan SK. 2022. Removal of copper, nickel, and zinc ions from an aqueous solution through electrochemical and nanofiltration membrane processes. *Applied Sciences* 12:280
25. Németh G, Mlinárik L, Török Á. 2016. Adsorption and chemical precipitation of lead and zinc from contaminated solutions in porous rocks: Possible application in environmental protection. *Journal of African Earth Sciences* 122:98–106
26. Zhang J, Lei Y, Hu S, Li X, Lin G, et al. 2023. Ultrasonic pretreatment-solvent extraction process for separating zinc from pickling waste liquid. *Journal of Environmental Chemical Engineering* 11(6):111160
27. Jayan N, Bhatlu MLD. 2021. Isolation and studies on zinc removal using microorganism from contaminated soil. *Materials Today: Proceedings* 44:1892–97
28. Carreira ARF, Passos H, Coutinho JAP. 2023. Metal biosorption onto non-living algae: a critical review on metal recovery from wastewater. *Green Chemistry* 25:5775–88
29. Ekmekyapar F, Aslan A, Bayhan YK, Cakici A. 2006. Biosorption of copper(II) by nonliving lichen biomass of *Cladonia rangiformis* hoffm. *Journal of Hazardous Materials* 137:293–98
30. Martins RJE, Pardo R, Boaventura RAR. 2004. Cadmium(II) and zinc(II) adsorption by the aquatic moss *Fontinalis antipyretica*: effect of temperature, pH and water hardness. *Water Research* 38(3):693–99
31. Prabhu S, Hegde S. 2022. Pteridophytes as effective biosorption agents of heavy metals. In *Ferns*, eds. Marimuthu J, Fernandez H, Kumar A, Thangaiah S. Singapore: Springer. pp. 651–70 doi: 10.1007/978-981-16-6170-9_28
32. Hegazy GE, Soliman NA, Ossman ME, Abdel-Fattah YR, Moawad MN. 2023. Isotherm and kinetic studies of cadmium biosorption and its adsorption behaviour in multi-metals solution using dead and immobilized archaeal cells. *Scientific Reports* 13:2550
33. Marković M, Gorgievski M, Štrbac N, Grekulović V, Božinović K, et al. 2023. Raw eggshell as an adsorbent for copper ions biosorption – equilibrium, kinetic, thermodynamic and process optimization studies. *Metals* 13:206
34. Imran-Shaukat M, Wahi R, Ngaini Z. 2022. The application of agricultural wastes for heavy metals adsorption: a meta-analysis of recent studies. *Bioresource Technology Reports* 17:100902
35. Simón D, Palet C, Costas A, Cristóbal A. 2022. Agro-industrial waste as potential heavy metal adsorbents and subsequent safe disposal of spent adsorbents. *Water* 14:3298
36. Shalaby MA, Matter IA, Gharieb MM, Darwesh OM. 2023. Biosorption performance of the multi-metal tolerant fungus Aspergillus sp. for removal of some metallic nanoparticles from aqueous solutions. *Heliyon* 9(5):e16125
37. Şenol ZM, Gül ÜD, Gurbanov R, Şimşek S. 2021. Optimization the removal of lead ions by fungi: explanation of the mycosorption mechanism. *Journal of Environmental Chemical Engineering* 9(2):104760
38. Oliveira AF, Machado RB, Ferreira AM, Sena IDS, Silveira ME, et al. 2023. Copper-contaminated substrate biosorption by *Penicillium* sp. isolated from kefir grains. *Microorganisms* 11(6):1439
39. Mushtaq S, Bareen FE, Tayyeb A. 2023. Equilibrium kinetics and thermodynamic studies on biosorption of heavy metals by metal-resistant strains of *Trichoderma* isolated from tannery solid waste. *Environmental Science and Pollution Research* 30(4):10925–54
40. Puranik PR, Paknikar KM. 1997. Biosorption of lead and zinc from solutions using *Streptoverticillium cinnamoneum* waste biomass. *Journal of Biotechnology* 55(2):113–24
41. El-Sayed MT. 2013. Removal of lead(II) by *Saccharomyces cerevisiae* AUMC 3875. *Annals of Microbiology* 63(4):1459–70
42. Kumar A, Tyagi A, Kumar S, Charaya MU, Singh R. 2023. An invasive plant *Ageratum houstonianum* L. as an adsorbent for the removal of triphenylmethane dye (malachite green): isotherm, kinetics, and thermodynamic studies. *Biomass Conversion and Biorefinery*
43. Langmuir I. 1918. The adsorption of gases on plane surfaces of glass, mica and platinum. *Journal of the American Chemical Society* 40:1361–403
44. Freundlich HMF. 1906. Over the adsorption in solution. *Journal of Physical Chemistry* 57:385–470 (in German)

45. Temkin MI, Pyzhev V. 1940. Kinetics of ammonia synthesis on promoted iron catalysts. *Acta Physiochim. URSS* 12:327–56
46. El-Gendy MMAA, Abdel-Moniem SM, Ammar NS, El-Bondkly AMA. 2023. Bioremoval of heavy metals from aqueous solution using dead biomass of indigenous fungi derived from fertilizer industry effluents: isotherm models evaluation and batch optimization. *BioMetals* 36:1307–29
47. Kumari S, Agrawal NK, Agarwal A, Kumar A, Malik N, et al. 2023. A prominent *Streptomyces* sp. biomass-based biosorption of zinc (II) and lead (II) from aqueous solutions: isotherm and kinetic. *Separations* 10(7):393
48. Olafadehan OA, Akpo OY, Enemuo O, Amoo KO, Abatan OG. 2018. Equilibrium, kinetic and thermodynamic studies of biosorption of zinc ions from industrial wastewater using derived composite biosorbents from walnut shell. *African Journal of Environmental Science and Technology* 12(9):335–56
49. Bueno DJ, Silva JO. 2014. Fungi: the fungal hyphae. In *Encyclopedia of Food Microbiology (Second Edition)*, eds. Batt CA, Tortorello ML. Oxford: Academic Press. pp. 11–19 doi: 10.1016/B978-0-12-384730-0.00132-4
50. Kapoor A, Viraraghavan T. 1997. Fungi as biosorbents. In *Biosorbents for Metal Ions*, eds. Wase J, Forster C. London: Taylor & Francis. pp. 67–85 doi: 10.3109/9780203483046
51. Delgado A, Anselmo AM, Novais JM. 1998. Heavy metal biosorption by dried powdered mycelium of *Fusarium flocciferum*. *Water Environment Research* 70(3):370–75
52. Hanif A, Bhatti HN, Hanif MA. 2009. Removal and recovery of Cu(II) and Zn(II) using immobilized *Mentha arvensis* distillation waste biomass. *Ecological Engineering* 35:1427–34
53. Danial AW, Dardir FM. 2023. Copper biosorption by *Bacillus pumilus* OQ931870 and *Bacillus subtilis* OQ931871 isolated from Wadi Nakheil, Red Sea, Egypt. *Microbial Cell Factories* 22:152
54. Nemeş LN, Bulgariu L . 2016. Optimization of process parameters for heavy metals biosorption onto mustard waste biomass. *Open Chemistry* 14(1):175–87
55. Jalija DO, Uzairu A, Ekwumemmgbo P. 2020. Biosorption of Zn (II) ions from aqueous solution by immobilized *Aspergillus fumigatus*. *Journal of Applied Sciences and Environmental Management* 23(11):1991–94
56. Ong DC, Pingul-Ong SMB, Kan CC, de Luna MDG. 2018. Removal of nickel ions from aqueous solutions by manganese dioxide derived from groundwater treatment sludge. *Journal of Cleaner Production* 190:443–51
57. Legorreta-Castañeda A, Lucho-Constantino C, Beltrán-Hernández R, Coronel-Olivares C, Vázquez-Rodríguez G. 2020. Biosorption of water pollutants by fungal pellets. *Water* 12:1155
58. Khodabakhshi A, Mohammadi-Moghadam F, Shakeri K, Hemati S. 2022. Equilibrium and thermodynamic studies on the biosorption of lead (II) by living and nonliving biomass of *Penicillium notatum*. *Journal of Chemistry* 2022:3109212
59. Wang J, Guo X. 2020. Adsorption isotherm models: classification, physical meaning, application and solving method. *Chemosphere* 258:127279
60. Babatunde KA, Negash BM, Jufar SR, Ahmed TY, Mojid MR. 2022. Adsorption of gases on heterogeneous shale surfaces: a review. *Journal of Petroleum Science and Engineering* 208:109466
61. Cherono F, Mburu N, Kakoi B. 2021. Adsorption of lead, copper and zinc in a multi-metal aqueous solution by waste rubber tires for the design of single batch adsorber. *Heliyon* 7(11):e08254
62. Batool F, Akbar J, Iqbal S, Noreen S, Bukhari SNA. 2018. Study of isothermal, kinetic, and thermodynamic parameters for adsorption of cadmium: an overview of linear and nonlinear approach and error analysis. *Bioinorganic Chemistry and Applications* 2018:3463724
63. Acharya A, Jeppu G, Girish CR, Prabhu B, Murty VR, et al. 2024. Adsorption of arsenic and fluoride: modeling of single and competitive adsorption systems. *Heliyon* 10(11):e31967
64. Edet UA, Ifelebuegu AO. 2020. Kinetics, isotherms, and thermodynamic modeling of the adsorption of phosphates from model wastewater using recycled brick waste. *Processes* 8(6):665
65. Xie S. 2024. Biosorption of heavy metal ions from contaminated wastewater: an eco-friendly approach. *Green Chemistry Letters and Reviews* 17:2357213
66. Sireesha C, Durairaj K, Balasubramanian B, Sumithra S, Subha R, et al. 2025. Process development of guava leaves with alkali in removal of zinc ions from synthetic wastewater. *Journal of the Taiwan Institute of Chemical Engineers* 166:105283
67. Allaoui M, Berradi M, Eddaoukhi A, Bensalah J, Dagdag O, et al. 2025. Evaluation of the efficiency of shell powder as a natural adsorbent for the adsorption of chromium in aqueous solutions: kinetic and thermodynamic approach and modeling of adsorption isotherms. *Journal of the Indian Chemical Society* 102(1):101503
68. Nag S, Das J, Biswas S, Lodh BK. 2025. Experimental and ANN based process optimization for bioremediation of Cr^{6+} and Cd^{2+} by green adsorbent prepared from *Artocarpus heterophyllus* leaves. *Journal of the Indian Chemical Society* 102(1):101485
69. Khare SK, Panday KK, Srivastava RM, Singh VN. 1987. Removal of victoria blue from aqueous solution by fly ash. *Journal of Chemical Technology and Biotechnology* 38(2):99–104
70. Başkan G, Açıkel Ü. 2024. Comparison of the bioaccumulation and biosorption of copper ions by *Rhizopus delemar* and *Candida lipolytica*. *Bioremediation Journal* 29:42–58
71. Mousa AM, Abdel-Galil, EA, Zhran M, Moussa MG. 2025. Biosorption performance toward Co(II) and Cd(II) by irradiated *Fusarium solani* biomass. *Environmental Geochemistry and Health* 47:47
72. Mubarak MF, Mohamed AMG, Keshawy M, ElMoghny TA, Shehata N. 2022. Adsorption of heavy metals and hardness ions from groundwater onto modified zeolite: batch and column studies. *Alexandria Engineering Journal* 61(6):4189–207
73. Wang J, Guo X. 2023. Adsorption kinetics and isotherm models of heavy metals by various adsorbents: an overview. *Critical Reviews in Environmental Science and Technology* 53:1837–65
74. Kumar PS, Ethiraj H, Venkat A, Deepika N, Nivedha S, et al. 2015. Adsorption kinetic, equilibrium and thermodynamic investigations of Zn(II) and Ni(II) ions removal by poly(azomethinethioamide) resin with pendent chlorobenzylidine ring. *Polish Journal of Chemical Technology* 17(3):100–9
75. Jaishankar M, Tseten T, Anbalagan N, Mathew BB, Beeregowda KN. 2014. Toxicity, mechanism and health effects of some heavy metals. *Interdisciplinary Toxicology* 7(2):60–72
76. Ortiz-Oliveros HB, Ouerfelli N, Cruz-Gonzalez D, Avila-Pérez P, Bulgariu L, et al. 2023. Modeling of the relationship between the thermodynamic parameters $\Delta H°$ and $\Delta S°$ with temperature in the removal of Pb ions in aqueous medium: case study. *Chemical Physics Letters* 814:140329
77. Ciobanu AA, Bulgariu D, Ionescu IA, Puiu DM, Vasile GG, et al. 2023. Evaluation of thermodynamic parameters for Cu(II) ions biosorption on algae biomass and derived biochars. *Symmetry* 15(8):1500
78. Alharbi NK, Al-Zaban MI, Albarakaty FM, Abdelwahab SF, Hassan SHA, et al. 2022. Kinetic, isotherm and thermodynamic aspects of Zn^{2+} biosorption by *Spirulina platensis*: optimization of process variables by response surface methodology. *Life* 12(4):585
79. Zarei S, Raanaei H, Mohammad-Hosseini V, Kamali S. 2025. Efficient removal of zinc ion pollution by carbon-based magnetic alloy: experimental, theoretical modeling and DFT studies. *Inorganic Chemistry Communications* 172:113735
80. Cobo AJM, Lozano FE, Vilar MM, Valenzuela CM, Ramos ER. 2025. Biotechnological applications of the ubiquitous fungus *Penicillium* sp. 8L2: biosorption of Zn(II) and synthesis of ZnO nanoparticles as biocidal agents. *Sustainability* 17(6):2379
81. Shobham, Bhanot V, Mamta, Kumar SK, Gupta S, et al. 2025. Unveiling the potential of *Aspergillus terreus* SJP02 for zinc remediation and its driving mechanism. *Scientific Reports* 15:3376
82. Abdelkarim MS, Ali MHH, Kassem DA. 2025. Ecofriendly remediation of cadmium, lead, and zinc using dead cells of *Microcystis aeruginosa*. *Scientific Reports* 15:3677
83. Raut PN, Dolas AS, Chougule SM, Darade MM, Murali G, et al. 2025. Green adsorbents for heavy metal removal: a study on zinc ion uptake by *Tinospora cordifolia* biocarbon. *Journal of Mines, Metals and Fuels* 73(1):21–25
84. Zhang X, Zhao C, Xue F, Xia B, Lu Y, et al. 2024. Adsorption of Zinc(II) Ion by Spent and Raw *Agaricus bisporus* in Aqueous Solution. *Processes* 12(4):717

85. Negi A, Joshi S, Joshi SK, Bhandari NS. 2024. Biosorption of zinc on functionally activated *Lantana camara* leaves: equilibrium, kinetic, and thermodynamic studies. *Biomass Conversion and Biorefinery*
86. Khalaf SA, Shartooh SM, Shihan MA. 2025. Assessing the loading capacity of walnut peels as a nanobiomass for the biosorption of certain heavy metals from wastewater. *Journal of Ecological Engineering* 26(2):169–82
87. Dharmadhas JS, Arumugam P, Periakaruppan R. 2023. Preparation and characterization of biosorbent *Sargassum myriocystum* for zinc removal. *Marine Biology Research* 19(2–3):121–31
88. Melčáková I, Růžovič T. 2021. Biosorption of zinc from aqueous solution using algae and plant biomass. *Nova Biotechnologica et Chimica* 10(1):33–43
89. Tiwari S, Aachhera S, Garg H, Rojra M, Nagar N, et al. 2022. Comparative biosorption kinetics study of Ni and Zn metal ions from the aqueous phase in sulfate medium by the wooden biomass of *Dalbergia sissoo*. *Environmental Quality Management* 31(4):63–73
90. Kalyani G, Gokulan R, Sujatha S. 2021. Biosorption of zinc metal ion in aqueous solution using biowaste of *Pithophora cleveana* Wittrock and *Mimusops elengi*. *Desalination and Water Treatment* 218:363–71
91. Ugwu EI, Agunwamba JC. 2020. Optimal conditions for adsorption of zinc from industrial wastewater using groundnut husk ash. *Environmental Monitoring and Assessment* 192:345
92. Chen SH, Cheow YL, Ng SL, Ting ASY. 2020. Bioaccumulation and biosorption activities of indoor metal-tolerant *Penicillium simplicissimum* for removal of toxic metals. *International Journal of Environmental Research* 14:235–42
93. Pérez-Marín AB, Ortuño JF, Aguilar MI, Lloréns M, Meseguer VF. 2024. Competitive effect of zinc and cadmium on the biosorption of chromium by orange waste. *Processes* 12(1):148
94. Feng CL, Li J, Li X, Li KL, Luo K, et al. 2018. Characterization and mechanism of lead and zinc biosorption by growing *Verticillium insectorum* J3. *PLoS One* 13(12):e0203859
95. Gaur N, Dhankhar R. 2009. Equilibrium modelling and spectroscopic studies for the biosorption of Zn^{+2} ions from aqueous solution using immobilized *Spirulina platensis*. *Iranian Journal of Environmental Health Science & Engineering* 6(1):1–6
96. El Sayed MT, El-Sayed ASA. 2020. Bioremediation and tolerance of zinc ions using *Fusarium solani*. *Heliyon* 6(9):e05048